Hydrodynamic Behavior of Biomass Micro-Particles in Counter-Flow Combustion of Dust Clouds

M. Akbari Vakilabadi[*], A. Binesh and M. Monfared

Malek-Ashtar University of technology, Tehran, Iran.

Abstract

A mathematical model is investigated in order to predict the effect of hydrodynamic forces, especially thermophoretic forces, on the micro-organic particles in counter-flow combustion in this research work. Hydrodynamic forces change the velocity and concentration of evaporative organic particles moving toward the flame, and they make a particle-free distance above the flame surface. Particle evaporation creates a thrust force that affects the velocity of the particles, which can be ignored compared to the other hydrodynamic forces. Also the temperature difference between the particles and the interaction of the particles on each other are neglected.

The distance between the inlet nozzle and the flame surface is divided into four zones in order to investigate the dynamic behavior of the particles in the flame front, and in each case, the dynamic particles equations are written, and the effects of thermophoretic force, weight force, drag force, and buoyant force are analyzed on the particles, and as a result, the velocity and concentration profiles of the particles are obtained in terms of distance from the flame front at different strain rates and with different particle diameters. The particle concentration of above the flame front increases with the balance of these forces, and increasing the particle accumulation above the flame decreases the combustibility of particles in the flame front. Then the length of the particle-free zone is extracted under the influence of different strain rates at different temperatures. As the flame surface approaches, the temperature gradient rises, and the thermophoretic force increases. Accordingly, the heavier particles accumulate closer to the flame surface.

Keywords: *Combustion, Counter-flow, Biomass dust clouds, Thermophoresis phenomenon.*

1. Introduction

The effect of heat gradient (i.e. thermophoretic force) on the dynamic behavior of particles is one of the most important phenomena in the combustion of organic dust-clouds, which has different applications in the aerosol technology field. Gomez and Rosner have experimentally investigated particle deflection in counter-flow combustion considering the thermophoretic effect. They concluded that the particles accumulated at a certain distance from the particle flame due to the thermophoretic force, and the particle concentration increased at that point. Particles' deposition has been experimentally investigated under the influence of thermophoresis [1]. The thermophoretic force in the combustion of dust-clouds causes the particles moving in the opposite direction of the heat gradient, which, in turn, has a great effect on the organic micro-particles. For this reason, the researchers have investigated the effect of thermophoretic force on the spherical

aerosols [2-5]. Amer et al. have studied the kinetics of combustion and pyrolysis of raw using the Ozawa-Flynn-Wall (OFW) method. They concluded that the samples pyrolyzed in 30 min had better results compared to the longer times [6]. Zuo et al. have improved the counter-flow combustion efficiency using a micro-compressor. They used hydrogen fuel in this new scheme. They concluded that the use of micro-compressor was suitable for the MTPV (micro thermo photovoltaic) system [7]. Yang et al. have modeled the biomass particles gasification, and compared them with sand particles. They concluded that the dispersion coefficient was much higher than sand particles [8]. In 2020, Peng et al. analyzed the hydrogen/air premixed combustion. They concluded that the amount of porous medium and C3H8 added should be sufficient to obtain a higher flame temperature in the combustor. The location of the flame also

depends on the amount of C3H8 added [9]. Karataş et al. have used a counter-flow combustion schemec to collect soot samples from methane-air flames in the 5-30 times compression range. They concluded that the diameter of the soot particles increased with increasing pressure. They also concluded that the particle density increased with increasing pressure [10]. Liu et al. have analyzed counter-flow combustion using the second law of thermodynamics. They studied the exergy losses in the combustion processes, and concluded that heat conduction was the dominant factor in exergy losses compared to other irreversible processes [11]. Malekian et al. have developed an effective method for analyzing the performance of micro-combustors. They modeled the diffusion flames using the asymptotic method, and concluded that with increasing heat recirculation coefficient, the flame location moveed towards the fuel nozzle, and the flame temperature rised [12]. Shi et al. have introduced a numerical model in order to simulate the preparation of TiO2 by the unmixed combustion of Ti (Titanium) particles in a counter-flow arrangement. They modeled the pre-heating, reaction, melting, and evaporation processes using the asymptotic concept. They concluded that heat loss could significantly shorten the distance between the stagnation plane and the flame front [13]. Gao et al. have determined the position of the flame front in oscillating combustion using a new experimental method. Their results showed that the flame area had a random fluctuation [14]. In a study, Azam et al. have examined the thermal decomposition behavior of fossil fuel (coal) combustion and solid waste such as municipal solid waste and waste-derived fuel. According to the models used in this study, fuels can be arranged in the order of activation energy as coal > waste fuel > municipal solid waste [15]. Biodiesel and biogas fuel as the promising alternative energy sources for dual-fuel diesel engines are attracting more researchers. Therefore, Oishi et al. have simulated the dual-burner performance of a diesel engine using biodiesel and biogas fuel. They concluded that the ratio of methane content in fuel had the greatest effect on the dual-burner thermal efficiency [16]. Cirillo et al. have proposed a new model for predicting the gasification of organic particles. In the model they developed, they modeled the performed thermophysical processes. The results are useful tools for analyzing the micro-CHP units' performance [17]. Wang et al. have proposed a new combined heat and power (CHP) system using biomass fuel based on the organic Rankin

cycle (ORC). They analyzed the output of the electrical power for different working fluids, and concluded that the fluid R141b could be the best option for CHP units [18]. In an experimental work, Zoladek et al. have performed an energy and economic analysis on a biomass power plant. They concluded that in the faraway rural areas, a biomass power plant could be used with a payback period between 1 to 15 years [19]. Falbo et al. have analyzed a new integrated energy system for small-scale combined heat and power (CHP) generation. The system includes a biodiesel internal combustion engine (ICE) and a supercritical organic Rankine cycle (SORC) to recover heat dissipation. They concluded by economic analysis that the payback period was 8.4 years [20]. Han et al. have performed a numerical simulation on the combustion of aluminum dust using the reactive Eulerin-Lagrangian method. In their numerical simulation analysis, they concluded that the constant burning rate was due to the exchange between the particle reaction surface and the maximum flame temperature. In addition, the flame structures were evaluated at different concentrations of aluminum and heterogeneous properties [21]. Yariv has studied the effect of temperature gradients on the spherical particle between two walls. They concluded that temperature changes increased with distance from the walls, while as Reynolds tends to zero, the profile becomes linear [22]. In 2015, Bidabadi et al. have investigated the effect of strain rate on the flame location on the counter-flow combustion of premixed dust-clouds. They concluded that as the strain rate increased, the flame location became closer to the stagnation plane [23]. In addition, Bidabadi et al. have studied the effect of heat loss and particle diameter on the counter-flow combustion of dust-clouds in an analytical study [24]. Jebeso et al. Have studied appropriate tree species for utilization of biomass energy by calculating trees' dry biomass and index of fuel value [25]. Pourkiaei et al. [26] have reviewed the current status, potential, and renewable energy applications in Iran. It is necessity to use renewable energy because of global warming issues and increasing greenhouse gas pollution, rising fossil fuel prices. Biomass energy is the third most important source for electricity generation and the most important source for thermal energy production among the various options [27]. The combustion modeling of biomass particles is complex due to the evaporation and reduction of the particle diameter as it approaches the flame surface. In 2012,

Monajat et al. examined the effect of moisture content in biomass particles on the flame velocity. They concluded that the flame velocity slowly decreased at a moisture content below 4%, and suddenly it increased at a moisture content upper than 5% [28]. Alaei et al. have investigated the environmental impact of biomass usage. They studied various sources of biomass. In different combinations of air and steam, and they concluded that the highest calorific value of the air-steam combination was 12.26 lb/s [29]. Alaei and Rperformed the chemical analysis of municipal wastewater in the Hamedan city, and estimated the calorific value of municipal wastewater to design a power plant with a suitable biomass fuel. They concluded that the maximum power generation was 3559.08 MW/month [30]. Alaei et al. have used the Hummer software to perform the economic and environmental analysis of a biomass power plant. They concluded that generating electricity using biomass reduced CO and CO2 emissions by 77.2 and 7.96 kg/year, respectively [31]. Alaei et al. have performed an energy-economic-environmental analysis for biogas production from waste. Using landfill software, they evaluated the methane production potential, and concluded that the amount of electricity generation per year was 11658.265MWh [32]. The effect of hydrodynamic forces, especially thermophoretic force, on the particles in counter-flow combustion of dust clouds has been investigated in this study. Figure 1 shows the plate flame from the counter-flow under the available assumptions. In the whole zone, the velocity of counter-flow is v = (ax, -ay), where a is the strain rate and the n_s/ρ ratio is assumed to be constant. If the strain rate is small, the problem can be solved one-dimensionally and only in the direction of the Y axis. The flame structure consists of three zones:

- Pre-heating zone, where the chemical reaction rate is small.

- Reaction zone, where the displacement term is negligible compared to the other terms.

- Post-flame zone, where the reaction rate comparable to other terms, is assumed to be negligible.

The main assumptions made are: (1) there is no temperature difference between the particles and the gaseous phase, (2) heterogeneous combustion (surface burning) is not possible, and we are dealing with a homogenous flame front, (3) constant properties, (4) diffusion coefficient is proportional to temperature squared, (5) the term $\frac{dU_{rel}}{dt}$ is replaced by $U_{rel}\frac{dU_{rel}}{dt}$ (6). In the whole zone, the velocity of counter-flow is v = (ax, - ay) and the $\frac{n_s}{\rho}$ ratio is assumed to be constant. (7) the flow is considered stable, (8) the phase flows are scattered in one phase, (9) the particles do not stick to each other, the initial number of particles is nu (number of particles per unit), and their initial radius, ru, is assumed clear, and (10) diffusion from pressure gradient is neglected. If the particles are motionless, the problem is like flowing through a porous environment, where a viscous force enters the particle surface through the movement of the surrounding gas.

If the ns value is small, it is likely that the fuel particles will burn with flames around each particle at any point in the reaction zone. In this study, nu is assumed to be enough large that the flames surrounding each particle are overlapped. It is shown in the references that if Φu is greater than 0.7 in the sprayed combustion, this is an overlap of the flames. This assumption can be approximately used for the combustion of dust-clouds. In this paper, Φu is assumed to be equal to one. The Zeldovich dimensionless number is defined as follows [33]:

$$Ze = \frac{E\,(T_f - T_u)}{R\,T_f^{\,2}} \tag{1}$$

We assumed that theZeldovich number was large in this study. The f and u indices indicate the conditions in the reaction zone and the pre-reaction zone (preheat), respectively.
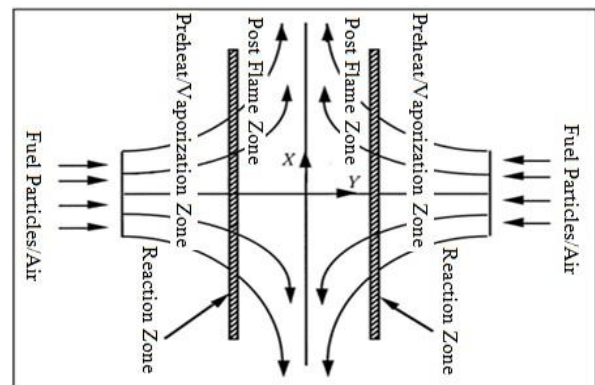
Figure 1. Schematic representation of pre-mixed counter-flow combustion with different zones.

2. Methodology

In this work, with a numerical-analytical method, the combustion of cloud particles in counter-flow schematic is first analyzed, and then the effect of thermophoretic force on the combustion of cloud particles is investigated. By reviewing the different references by the authors, no research has so far investigated the effect of thermophoretic force on the counter-flow

combustion of cloud particles analytically (or numerically). In this work, first, the governing equations of the cloud particles combustion in a counter-flow schematic are driven (Equations 2 to 11), and then non-dimensionalize the equations with selecting appropriate dimensionless parameters (Equations 16 to 31). Using the momentum equation, the effect of the thermophoretic force, which was caused due to the difference in temperature between the flame front and its surroundings, was investigated (particle dynamic section). In the cloud particle combustion, it is important to analyze the particle velocity and particle accumulation rate before they ignite.

3. Governing equations

In obtaining the conservation equations, we assume that the diffusion coefficient, D, is proportional to T and the coefficient of mixture thermal conductivity, k, to be constant. We also assume that ρ_v and ρ_T are constant with concerning to the continuity law and the state equation, respectively, where ρ and v are the density and velocity of the mixture, respectively, which we assumed to be equal to -aY.

3.1. Mass conservation equation

The equation for the mass conservation of the gas phase in counter-flow is as follows:

$$-aY \frac{dY_F}{dY} = D_F \frac{D^2Y_F}{dY^2} - \frac{\omega_F}{\rho} \tag{2}$$

ω_F is the reaction rate that we define as follows [34]:

$$\omega_F = \rho Y_F B e^{\frac{-E}{RT}} - \rho Y_P B' e^{-E'/RT} \tag{3}$$

In the above equation, ρ, Y_F, Y_P, R, B, E, T, B', and E' express the density, fuel mass fraction, product mass fraction, global gas constant, pre-exponential factor, activation energy of forward reaction, temperature, pre-exponential factor, and activation energy of the backward, respectively.

3.2. Particle conservation equations

The particle conservation equation in counter-flow combustion is written as follows:

$$aY \frac{dY_s}{dY} = \frac{\dot{\omega}_{vap}}{\rho} \tag{4}$$

where a is the strain rate and ρ is the density of the particles and gas mixture. Y_s and $\dot{\omega}_{vap}$ are the

mass ratio and the evaporation rate of the particles, respectively, and are defined as follow:

$$Y_s = \frac{m_p}{m_o} = \frac{r_p^3 n_s}{r_u^3 n_u} \tag{5}$$

$$\dot{\omega}_{vap} = A n_s 4 \pi r^2 T^n H\left(T - T_v\right) \tag{6}$$

In this equation, m_o, T_v, T, and H are the initial mass of the particle, evaporation temperature of the particle, mixture temperature, and Heaviside function, respectively.

3.3. Gas-phase equation

By writing the gas phase equations on the Euler's view, these equations include a source of solid phase. The governing conservation equations in the low Mach numbers are as follow:

$$-aY \frac{dY_F}{dY} = D_F \frac{D^2Y_F}{dY^2} - \frac{\omega_F}{\rho} + \frac{\omega_{vap}}{\rho} \tag{7}$$

$$aY \frac{dY_s}{dY} = \frac{\omega_{vap}}{\rho} \tag{8}$$

$$-aY \frac{dT}{dY} = D_T \frac{d^2T}{dY^2} + \omega_F \frac{Q}{\rho c} - \omega_{vap} \frac{Q_{vap}}{\rho c} \tag{9}$$

In the energy equation, the heat capacity is defined as follows:

$$C = Cg + \frac{4\pi r^3 C_s \rho_s n_s}{3\rho} \tag{10}$$

where C_g and C_s are the heat capacity of the gas and the particle, respectively.

3.4. Energy conservation equation

In the counter-flow, we write the energy conservation equation as follows:

$$-aY \frac{dT}{dY} = D_T \frac{d^2T}{dY^2} + \omega_F \frac{Q}{\rho c} - \omega_{vap} \frac{Q_{vap}}{\rho c} \tag{11}$$

where D_T is the heat diffusion coefficient and C is the heat capacity of the mixture, which is defined as follows [33]:

$$\omega_{vap} = A n_s 4 \pi r^2 T^n \tag{12}$$

In equation (12), it is assumed that A and n are clear, T is the gas temperature, and it is assumed that the particle temperature is approximately equal to the gas temperature. Since the evaporation rate increases with increasing

temperature, so it is expected that the evaporation near the reaction zone is more significant than the other zones; then it is assumed that for each $\frac{T_f - T_u}{T_f}$ > 1, the evaporation rate in equation (11) is proportional to $(T - T_u)^n$ [33].

3.5. Boundary conditions on conservation equations
In $Y \rightarrow +\infty$, we have:

$$Y_F = 0 , \quad T = T_u , \quad Y_s = Y_{FU} \tag{13}$$

In $Y = Y *$, we have:

$$
\begin{aligned}
Y_F &= 0 \\
Y_s &= 0
\end{aligned} \tag{14}
$$

4. Non-dimensionalization of governing equations
We define the dimensionless parameters as follow:

$$
\begin{cases}
y_F = \dfrac{Y_F}{Y_{FC}} \\[2mm]
\Theta = \dfrac{T - T_u}{T_f - T_u} \\[2mm]
y_s = \dfrac{Y_s}{Y_{FC}} \\[2mm]
y = \dfrac{Y}{L}
\end{cases} \tag{15}
$$

where Y_{FC} and T_f are the values corresponding to the chemical equilibrium given by the following equations.
The quantity Y_{Fc} is selected in such a way that:

$$Y_{FC}Q = C(T_f - T_u) \tag{16}$$

The propagation velocity (slow flame velocity) can be expressed as the following equation [12]:

$$S_L = \left[\frac{2[Le_F + re^{-\alpha\psi}(Le_p + \alpha^2\psi)]}{\beta^2} D_T Be^{-\frac{E}{RT_f}} \right]^{\frac{1}{2}} \tag{17}$$

In equation (19), L is the thickness of the mixed layer and is equal to:

$$L = \sqrt{\frac{2D_T}{a}} \tag{18}$$

Also Le_F, Le_P, and ϵ are the Lewis number of the gas fuel, dimensionless strain rate, and Lewis number of the products are as follow, respectively:

$$\grave{o} = \frac{D_T}{L\,S_L} \tag{19}$$

$$Le_F = \frac{D_T}{D_F} \tag{20}$$

The parameters of the above equation are:

$$
\begin{aligned}
\psi &\equiv (E' - E) / R(T_e - T_u) \\
\alpha &\equiv (T_e - T_u)/T_e
\end{aligned} \tag{21}
$$

$$r = \frac{B'}{B} \tag{22}$$

The Zeldovich number (the dimensionless activation energy of the forward reaction) [12]:

$$\beta = E(T_e - T_u)/RT_e^2 \tag{23}$$

The variable y_s can be rewritten as follows:

$$y_s = \frac{Y_s}{Y_{FC}} = \frac{n_s 4\pi r^3 \rho_s}{3\rho Y_{FC}} \tag{24}$$

As mentioned earlier, it is assumed that $\frac{n_s}{\rho}$ is a constant value, and therefore:

$$\frac{n_s}{\rho} = \frac{n_u}{\rho_u} \tag{25}$$

4.1. Dimensionless reaction rate

$$
\omega = \frac{2\omega_F}{aY_{FC}} = \\
\frac{\beta^2}{2\left[Le_F + r\,e^{-\alpha\psi}\left(Le_P + \alpha^2\psi\right)\right]}\,\varphi\exp\left(\frac{\beta(\theta-1)}{1+\alpha(\theta-1)}\right) \tag{26}
$$

In the above equation:

$$\varphi = y_F + re^{-\alpha\psi} - ry_p \exp\left(\frac{-\alpha\psi}{1+(\theta-1)}\right) \tag{27}$$

When r = 0, the above equation becomes the irreversible state reaction rate.
Now, according to the above equation and the equation $Y_{FC} = Y_{Fu} - Y_{Fe}$, we have:

$$-2y\frac{dy_F}{dy} = \frac{1}{Le_F}\frac{d^2y_F}{dy^2} - \omega\,\grave{o}^{-2} + \gamma_1 y_s^{\frac{2}{3}}\theta^n \tag{28}$$

where:

$$\gamma_1 = \frac{9.67 \ A \ n_u^{\frac{1}{3}} \left(T_f - T_u\right)^n}{a Y_{FC}^{\frac{1}{3}} \rho_u^{\frac{1}{3}} \rho_s^{\frac{2}{3}}} \tag{29}$$

4.2. Energy conservation equation

Assuming that the heat from evaporation of particles is negligible, we have:

$$-2 \ y \frac{d\theta}{dy} = \frac{d^2\theta}{dy^2} + \omega \ \grave{o}^{-2} \tag{30}$$

4.3. Solid particle mass conservation equation

Using the dimensionless parameters, we make dimensionless the particles mass conservation equation as follows:

$$2 \ y \frac{dy_s}{dy} = \gamma_1 y_s^{\frac{2}{3}} \ \theta^n \tag{31}$$

The boundary conditions in the dimensionless state:

$$y \to \infty \begin{cases} \theta = 0 \\ y_F = 0 \\ y_s = \dfrac{Y_{Fu}}{Y_{FC}} \end{cases} \tag{32}$$

$$y = y^* \to \begin{cases} y_s = 0 \\ y_f = 0 \end{cases} \tag{33}$$

5. Problem analysis

5.1. Pre-heat zone

In the condition $Z < Z^*$ (where Z^* indicates the flame location), we have the pre-heat zone.

The chemical reaction between the gas fuel and the oxidizer is negligible at Ze→∞. Then by putting $\omega = 0$ in equation (30) and the boundary conditions (32) and (33), the solution is as follows:

$$\theta = \frac{1 - \mathrm{erf}\left(z\right)}{1 - \mathrm{erf}\left(z^*\right)} \tag{34}$$

where erf (x) is an error function, and defined as follows:

$$\mathrm{erf}\left(x\right) = \frac{2}{\sqrt{\pi}} \int_0^x e^{-t^2} dt \tag{35}$$

Given to the following, mutation conditions, the necessary condition for satisfying the continuity on both sides of the reaction zone is obtained [33].

$$\left[\frac{d\theta}{dy}\right]_{y^{*+}} + \left[\frac{dy_F}{dy}\right]_{y^{*+}} = \left[\frac{d\theta}{dy}\right]_{y^{*-}} + \left[\frac{dy_F}{dy}\right]_{y^{*-}} \tag{36}$$

Assuming that the in y^{*+} changes in y can be ignored, then:

$$\left[\frac{d\theta}{dy}\right]_{y^{*-}} + \left[\frac{dy_F}{dy}\right]_{y^{*-}} = 0 \tag{37}$$

6. Particle dynamics in pre-heat and evaporation zone

In the Lagrange's view, the Brownian motion is ignored, and the particle path (location and velocity in time) is obtained by integrating the following differential equation:

$$\frac{d\left(m_p U_p\right)}{dt} = \sum F \tag{38}$$

The different forces acting on the particle in pre-heat and evaporation zones are defined as follow:

6.1. Gravity force

A particle can be affected by the gravity force; the value is proportional to the particle weight. The gravity force for a spherical particle is written as follows:

$$F_g = \frac{4\pi}{3} r_p^{\ 3} \rho_p g \tag{39}$$

where r_p and ρ_p are the particle radius and density, respectively.

6.2. Bouyancy force

As we assume that the particle is completely submerged in the gas phase, a bouyancy force that is in the opposite direction of gravity is applied to the particle. The bouyancy force is written as follows:

$$F_{bouyancy} = \rho_g \frac{4}{3} \pi r_p^{\ 3} . g \tag{40}$$

where ρ_g is the surrounding gas density.

6.3. Drag force

When a particle moves at a different speed than the gas around it, a resistive force is applied to it that it is in the opposite direction of the particle's motion. In low Reynolds numbers, the drag force

applied to a particle with diameter r_p is as follows:

$$F_D = -6\pi\mu r_p U_{rel} \tag{41}$$

where μ and U_{rel} are the gas viscosity and the relative velocity, respectively.

6.4. Thermophoretic force

By assuming that the Nodson number is small, the Boltzmann equation becomes the Navier-Stokes equation, and the thermophoretic force is written as follows:

$$F_{th} = -24\pi\mu^2 r_p C_s \frac{k_g}{k_p + 2k_g} \frac{\nabla T}{\rho_g T_m} \tag{42}$$

The best value for C_s is 1.17 [35]. The term d/dt is replaced by $U_p\left(\frac{d}{dx}\right)$ in Equation (38) to find the concentration and velocity in terms of distance from the flame.

6.5. Particle volume ratio

As shown in the following figure, a control volume that is large enough in the flame front containing a number of particles is used to calculate the particle density or particle volume ratio. The particle path is vertical in the control volume. The change in particle density that passes through this control volume is obtained from the flux balance of the mass that enters and leaves the control volume. The density is considered as the ratio of mass to volume at each point for a continuous environment. However, in one flow, the two-phase of the solid and gas is in the form of the volume ratio of each phase, called the apparent density.

$$\psi = \frac{V_p}{V} = \frac{n_s m_o Y_s}{\rho_p} \tag{43}$$
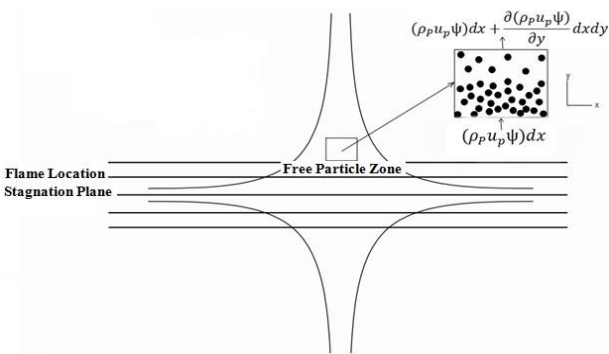
Figure 2. Changes on ratio of particle volume to control volume.

The mass conservation equation can be written as follows:

$$\frac{\partial\left(\rho_p U_{rel}\psi\right)}{\partial x} = \dot{\omega}_{vap} \tag{44}$$

where U_{rel} is the relative velocity; it means that the velocity of the particles into burning velocity on the combustion location is located at the leading edge:

$$U_{rel} = U_p - v_v \tag{45}$$

By combining Equations (5) and (43), the particle radius is obtained from the following equation:

$$r_p = \sqrt[3]{\frac{n_u m_o}{\rho_p} \frac{Y_s^2}{\psi}} r_u \tag{46}$$

According to the forces acting on a particle in the counter-low combustion, we obtain the momentum conservation equation as follows:

$$F_{drag} - F_{thermophoretic} + F_{gravity} - F_{bouyancy} = m_p \ddot{y} \tag{47}$$

Each one of the above forces has already been described.

6.6. Particle dynamics

The thermophoretic force can be assumed to be negligible at a certain distance from the flame. This distance is obtained using the results of Han *et al.* [36] from the following equation:

$$y_e = \left(\frac{\rho_p}{m_o n_u}\right)^{0.1} \left(\frac{\rho_g v_f C}{k_g} D\right)^{0.2} y_v \tag{48}$$

6

Therefore, the zone before the flame can be divided into four parts: the first zone $-\infty < y < y_e$, the second zone $y_e < y < y_v$, the third zone $y_v < y < y_{free\ particle}$, and the fourth zone $y_{free\ particle} < y < y_{flame}$.

As it approaches the flame surface, the value of thermophoretic force increases, so at one point, the velocity of the particles becomes zero, and they can no longer approach the surface of the flame more than that distance. From this expression, we can obtain $y_{free\ particle}$. After putting zero for the value of the particle velocity, we will have:

$$
L_{free\,particle} =
$$

$$
\sqrt{-ln\left(\frac{\left(k_p + 2k_g\right)\left(r_p T_m\right)\left[\sqrt{p}\left(erf\left(y^*\right)-1\right)r_p^2 g\left(r_p - r_g\right)\right]}{12m_s^2 C_s k_g}\right)} \quad (49)
$$

● $-\infty < y < y_e$

At this given length, according to the balance between the forces of drag, buoyancy, and gravity, the particles move at a constant velocity, this value is obtained as follows:

$$
F_D + F_B = F_g \quad (50)
$$

where, by placing the relevant values, we will have:

$$
U_p = \frac{2}{9}\frac{r_p^2 g}{\mu}\left(\rho_p - \rho_g\right) \quad (51)
$$

It is clear that the particles volume ratio at this distance is constant and its value is as follows:

$$
\psi_u = \frac{n_u m_o}{\rho_p} \quad (52)
$$

● $y_e < y < y_v$

The thermophoretic force is dominant in this zone, and it can be assumed that the other forces acting on the particle are balanced with each other. Therefore, the momentum equation is as follows:

$$
24\pi\mu^2 r_p C_s \frac{1}{m_p}\frac{k_g}{k_p + 2k_g}\frac{\nabla T}{\rho_g T_m} = U_p \frac{dU_p}{dy} \quad (53)
$$

By solving the above equation, we have:

$$
U_p = \sqrt{48\pi\mu^2 r_p C_s \frac{k_g}{k_p + 2k_g}\frac{1}{\rho_g T_m}\left(\frac{1-\mathrm{erf}\left(y\right)}{1-\mathrm{erf}\left(y^*\right)}\right)+C} \quad (54)
$$

According to the boundary conditions, at $y = y_e$, the particle velocity is equal to $U = \frac{2}{9}\frac{r_p^2 g}{\mu}\left(\rho_p - \rho_g\right)$

Therefore, the value of C is equal to:

$$
C = \frac{2}{9}\frac{r_p^2 g}{\mu}\left(\rho_p - \rho_g\right) - \sqrt{48\pi\mu^2 r_p C_s \frac{k_g}{k_p + 2k_g}\frac{1}{\rho_g T_m}\left(\frac{1-\mathrm{erf}\left(y_e\right)}{1-\mathrm{erf}\left(y^*\right)}\right)} \quad (55)
$$

For the concentration of solid particles according to figure 9-11 in this zone, we have:

$$
\psi = \frac{C_1 y}{\rho_p U_p} \quad (56)
$$

which we obtain C_1 with regard to the boundary conditions at $y = y_v$.

$$
in \quad y = y_v \quad \rightarrow \begin{cases} \psi = \psi_u \\ U = U_o \end{cases} \quad (57)
$$

Therefore, $C_1 = \frac{\rho_p U_o \psi_u}{y_e}$.

● $y_v < y < y_{free\,particle}$

Now, in the evaporation zone, $y_v < y < y_{free\,particle}$, given the evaporation of the particles occurs and the mass and the diameter of the particles decrease, so before solving the equations, we must obtain the mass and the diameter of the particles in terms of particle concentration (y_s).

$$
r_p = \sqrt[3]{\frac{n_u m_o}{\rho_p}\frac{y_s^2}{\psi}} r_u \quad (58)
$$

$$
m_p = \frac{m_o n_u}{n_s} y_s \quad (59)
$$

Therefore:

$$
\rho_s \frac{4}{3}\pi r_p^3 \cdot \ddot{y}_p - f\cdot\dot{y}_p =
$$
$$
f\left(\vartheta\frac{K}{T}\cdot\nabla T\right) -
$$
$$
\rho_s \frac{4}{3}\pi r_p^3 \cdot g -
$$
$$
f\cdot V_{gas} + \rho_g \frac{4}{3}\pi r_p^3 \cdot g \quad (60)
$$

which it can be more summarized as follows:

$$
24\pi\mu^2 r_p C_s \frac{k_g}{k_p + 2k_g}\frac{\nabla T}{\rho_g T_m} = U_p \frac{d(m_p U_p)}{dy} \quad (61)
$$

By solving the particle mass conservation equation:

$$y_s =$$

$$\left(\frac{\gamma_1}{6\left(1-\mathrm{erf}\left(y^*\right)\right)} \right)^3 \begin{bmatrix} 1.02\,y^6 - 4*10^{-4}\,y^5 - \\ 7.5*10^{-3}\,y^4 - \\ 6.7*10^{-2}\,y^3 - \\ 0.36\,y^2 - 1.46\,y + \\ 0.97*\ln\left(|y|\right) \end{bmatrix}^3 \tag{62}$$

The particle concentration can be obtained from the following equation:

$$\psi =$$

$$\frac{3\rho Y_{FC}}{\rho_s^2 \cdot r} \cdot \frac{1}{u_p} \cdot \int y_s \left(\frac{1-\mathrm{erf}(y)}{1-\mathrm{erf}\left(y^*\right)} \right) dy =$$

$$\frac{3\rho Y_{FC}}{\rho_s^2 \cdot r} \cdot \frac{1}{u_p} \cdot$$

$$[\int \left(\left(\frac{\gamma_1}{6\left(1-\mathrm{erf}\left(y^*\right)\right)} \right)^3 \left[1.02\,y^6 - 4*10^{-4}\,y^5 - \\ 7.5*10^{-3}\,y^4 - 6.7*10^{-2}\,y^3 - 0.36\,y^2 - 1.46\,y + 0.97*\ln\left(|y|\right) \right]^3 \right)$$

$$\cdot \left(\frac{1-\mathrm{erf}(y)}{1-\mathrm{erf}\left(y^*\right)} \right) dy] \tag{63}$$

By numerically solving the equations (61) and (63), the velocity and concentration of the particles can be obtained at the third zone, respectively.

7. Results and discussion

As the flame structure depends on the particles behavior, it is necessary to state the motion of the particles near the flame to explain the particle flame propagation mechanism. Therefore, the changes in particle velocity and density as well as the flame temperature, location and the particle-free length related to organic micro-particles were theoretically analyzed in this study. This study is based on the use of the particle motion's Lagrange equation and effective forces such as thermophoretics, gravity, drag and bouyancy to explain and analyze the particle motion. As it can be seen in this study, the particles first approach the surface of the flame at a constant speed, then at a certain distance from the flame; the particle velocity decreases at a certain distance due to the thermophoretic force on the particle, so the velocity reaches zero at a certain point and the particle concentration increases there. Next, a control volume above the combustion location is considered to estimate the density profile of the organic micro-particles.

The particle-free length changes of the flame surface in terms of the flame surface temperature changes at different particle diameters shown in figure 3. As it can be seen in the figure, the particle-free length decreases with increasing particle diameter, and the particle-free length increases with increasing flame temperature. The reason that the particle-free length decreases with increasing the particle diameter is that the force of the particle's weight increases, and as a result, it travels a greater distance to be dominated by the thermophoretic force and to stop the particle. Obviously, as the temperature of the momentum flame entering the surrounding gas molecules increases, when the gas molecules hit the particle surface, more momentum enters the particle, thus increasing the stopping distance of the particles from the flame surface. In this figure, the effect of thrust that is generated due to particles evaporation is not considered. The particle-free length changes in terms of strain rate at different flame temperature values shown in Figure 4. As it is known, the strain rate increases because the rate of change of particle velocity is high at a certain temperature, then the particles have a more acceleration, and consequently, more inertial force, so at a closer distance from the flame surface, the thermophoretic force dominates it and stops the particle, which reduces the particle-free length.

The temperature difference between the particles is ignored, and all of them are considered isothermal. Obviously, in fact, there is a temperature difference between the particles but the effect of this difference on the particle-free distance is small. The changes in particle velocity above flame location are shown in Figure 5. We can see that as the strain rate increases, the particles tend to stop closer to the flame surface. The reason for this phenomenon is that the force of inertia and the weight are higher than the thermophortic force for particles with larger diameters. As it can be seen, the thrust force has little effect on the particle stagnation point, and can be ignored. The particle-free distance changes are plotted in terms of particle diameter changes in Figure 6. As it can be seen, as the particle diameter increases due to the gravitational force increases, the thermophoretic force dominates the gravitational force at a closer distance from the flame, and this causes the particle concentration increases in that zone. If the strain rate is assumed to be very low, the results should be equal to the pre-mixed combustion of the particles. Han *et al.* [36] have experimentally investigated the effect of thermophoretic force on the particles in the pre-mixed flow combustion, and our results are in good agreement with the Han's experimental results. We can see this correspondence in figure 7.
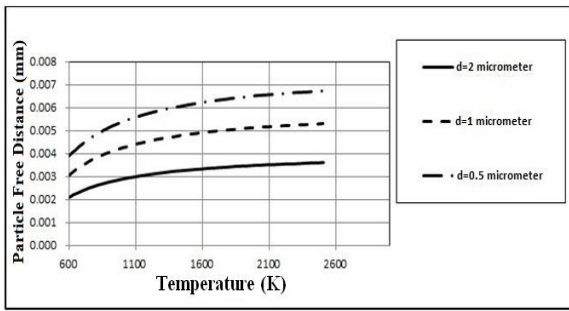
Figure 3. Particle- free zone changes in temperature at different particle diameters.
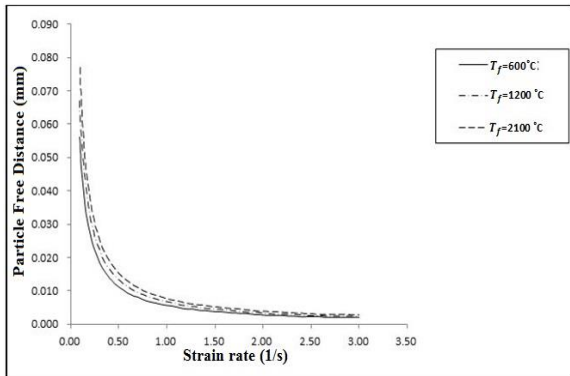
Figure 4. Effect of the strain rate on particle-free zone at different flame temperatures.
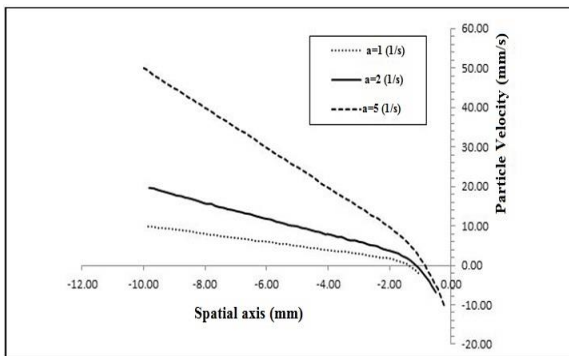
Figure 5. Particle velocity changes above flame surface at different strain rates.
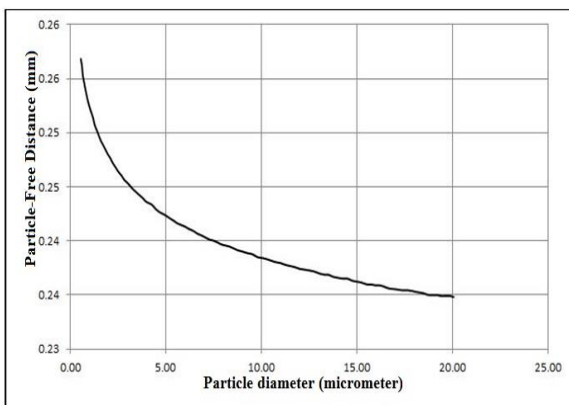
Figure 6. Changes in particle-free distance versus particles diameter.
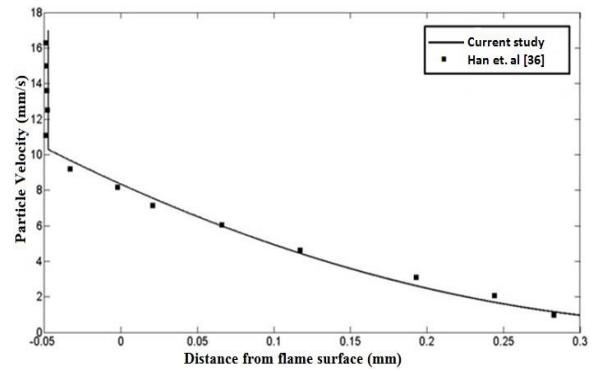
Figure 7. Changes in particle velocity at low strain rates in current study *vs.* experimental result measured by Han *et al.*

8. Conclusion

The changes in the micro-particles organic velocity, micro-particles density, flame temperature, flame location, and particle-free length were theoretically analyzed in this study. After extracting the governing equations of counter-flow combustion of the dust clouds, using the Lagrange equation, particle motion, and the hydrodynamic forces affecting particles such as thermophoretic, gravity, drag and buoyancy, particle motion at different flame temperature states, and different strain rates was analyzed. As the particles approach the surface of the flame, the thermophoretic force increases, and at a certain distance, an equilibrium is created between the thermophortic force and the gravity. At this point, the particles stop and accumulate there and as a result; the volume fraction of particles reaches the maximum value. The particle size strongly affects the hydrodynamic behavior of particles, which decreases with increasing particle diameter. The results of this model can be used to prevent unwanted explosions in the flammable particle storerooms. These results are also very useful for more completing the computer codes such as [37] (particle combustion simulation code) to simulate flame propagation in the explosion of micro-organic particles.

9. References

[1] N. Montassier, D. Boulaud, and A. Renoux. Experimental study of thermophoretic particle deposition in laminar tube flow. Journal of Aerosol Science. 22 (1991) 677-87.

[2] B. Vasu, R.S.R. Gorla, and P. Murthy. Thermophoresis on boundary layer heat and mass transfer flow of Walters-B fluid past a radiate plate with heat sink/source. Heat and Mass Transfer. 53 (2017) 1553-70.

[3] T. Grosan, R. Pop, and I. Pop. Thermophoretic deposition of particles in fully developed mixed

convection flow in a parallel-plate vertical channel. Heat and mass transfer. 45 (2009) 503-9.

[4] M. Partha. Thermophoresis particle deposition in a non-Darcy porous medium under the influence of Soret, Dufour effects. Heat and mass transfer. 44 (2008) 969-77.

[5] S. Asiaei, V. Darvishi, M.H. Davari, D. Zohrevandi, and H. Moghadasi. Thermophoretic isolation of circulating tumor cells, numerical simulation and design of a microfluidic chip. Journal of Thermal Analysis and Calorimetry. 137 (2019) 831-9.

[6] M. Amer, P. Brachi, G. Ruoppolo, I. El-Sharkawy, M. Ahmed, S. Ookawara, *et al*. Pyrolysis and combustion kinetics of thermally treated globe artichoke leaves. Energy Conversion and Management. 246 (2021) 114656.

[7] W. Zuo, Q. Li, Z. He, and Y. Li. Numerical investigations on thermal performance enhancement of hydrogen-fueled micro planar combustors with injectors for micro-thermophotovoltaic applications. Energy. 194 (2020) 116904.

[8] S. Yang, H. Wang, Y. Wei, J. Hu, and J.W. Chew. Particle-scale modeling of biomass gasification in the three-dimensional bubbling fluidized bed. Energy conversion and management. 196 (2019) 1-17.

[9] Q. Peng, W. Yang, E. Jiaqiang, Z. Li, H. Xu, G. Fu, *et al*. Investigation on H_2/air combustion with C_3H_8 addition in the combustor with part/full porous medium. Energy Conversion and Management. 228 (2021) 113652.

[10] A.E. Karataş, B. Gigone, and Ö.L. Gülder. Soot aggregate morphology deduced from thermophoretic sampling in coflow laminar methane diffusion flames at pressures up to 30 bar. Combustion and Flame. 222 (2020) 411-22.

[11] Y. Liu, J. Zhang, D. Ju, L. Shi, and D. Han. Second-law thermodynamic analysis on non-premixed counterflow methane flames with hydrogen addition. Journal of Thermal Analysis and Calorimetry. 139 (2020) 2577-83.

[12] N. Malekian, H. Moghadasi, and M. Bidabadi. An asymptotic approach to heat recirculation in diffusion flames fueled by organic particles. Journal of Thermal Analysis and Calorimetry. 145 (2021) 2363-77.

[13] Z. Shi, A.M. Ranjbar, S. Shayanseresht, K.D. Narooei, M.T. Fouladvand, L. Deng, *et al*. Numerical modeling of non-premixed combustion of micron-sized Ti particles in counter-flow arrangement: The effects of heat losses. Sustainable Energy Technologies and Assessments. 45 (2021) 101106.

[14] L. Gao, S. Peng, X. Huang, Y. Kang, S. Su, M. Sun, *et al*. A novel method for the identification of flame front's position on thermoacoustic coupling combustion oscillations. Energy Science & Engineering. 9 (2021) 1872-86.

[15] M. Azam, S.S. Jahromy, W. Raza, C. Jordan, M. Harasek, and F. Winter. Comparison of the combustion characteristics and kinetic study of coal, municipal solid waste, and refuse- derived fuel: Model- fitting methods. Energy Science & Engineering. 7 (2019) 2646-57.

[16] Y. Oishi, R.S. Situmorang, R.A. Sembiring, H. Kawai, and H. Ambarita. Performance, rate of heat release, and combustion stability of dual- fuel mode in a small diesel engine. Energy Science & Engineering. 7 (2019) 1333-51.

[17] D. Cirillo, M. Di Palma, M. La Villetta, A. Macaluso, A. Mauro, and L. Vanoli. A novel biomass gasification micro-cogeneration plant: Experimental and numerical analysis. Energy Conversion and Management. 243 (2021) 114349.

[18] Q. Wang, W. Wu, and Z. He. Thermodynamic analysis and optimization of a novel organic Rankine cycle-based micro-scale cogeneration system using biomass fuel. Energy Conversion and Management. 198 (2019) 111803.

[19] M. Żołądek, R. Figaj, and K. Sornek. Energy analysis of a micro-scale biomass cogeneration system. Energy Conversion and Management. 236 (2021) 114079.

[20] L. Falbo, D. Perrone, P. Morrone, and A. Algieri. Integration of biodiesel internal combustion engines and transcritical organic Rankine cycles for waste-heat recovery in small scale applications. International Journal of Energy Research. (2021).

[21] D.-H. Han, and H.-G. Sung. A numerical study on heterogeneous aluminum dust combustion including particle surface and gas-phase reaction. Combustion and Flame. 206 (2019) 112-22.

[22] E. Yariv. Thermophoresis due to strong temperature gradients. SIAM Journal on Applied Mathematics. 69 (2008) 453-72.

[23] M. Bidabadi, M.A. Vakilabadi, and A. Esmaeilnejad. Strain rate effect on microorganic dust flame in a premixed counterflow. Heat Transfer Research. 46 (2015).

[24] M. Bidabadi, M.A. Vakilabadi, A.K. Poorfar, E. Monteiro, A. Rouboa, and A. Rahbari. Mathematical modeling of premixed counter-flow combustion of organic dust cloud. Renewable Energy. 92 (2016) 376-84.

[25] G. Jebeso, M. Fekadu, and T. Dejene. Above-ground Biomass and Fuel Value Index of Selected Tree Species for Fuelwood Production in Ethiopia. (2014).

[26] P. S Mohsen, F. Pourfayaz, R. Shirmohamadi, S. Moosavi, and N. Khalilpoor. Potential, current status, and applications of renewable energy in energy sector of Iran: A review. Renewable Energy Research and Applications. 2 (2021) 25-49.

[27] L. Nunes, J. Matias, and J. Catalão. Mixed biomass pellets for thermal energy production: A review of combustion models. Applied Energy. 127 (2014) 135-40.

[28] N.F. Munajat, C. Erlich, R. Fakhrai, and T.H. Fransson. Influence of water vapour and tar compound on laminar flame speed of gasified biomass gas. Applied energy. 98 (2012) 114-21.

[29] R. Alayi, E. Sobhani, and A. Najafi. Analysis of environmental impacts on the characteristics of gas released from biomass. Anthropogenic Pollution. 4 (2020) 1-14.

[30] R. Alayi and H. Rouhi. Techno-economic analysis of electrical energy generation from urban waste in Hamadan, Iran. International Journal of Design & Nature and Ecodynamics. 15 (2020) 337-41.

[31] R. Alayi, M. Jahangeri, and H. Monfared. Optimal location of electrical generation from urban solid waste for biomass power plants. Anthropogenic Pollution. 4 (2020) 44-51.

[32] R. Alayi, M. Sadeghzadeh, M. Shahbazi, S.R. Seyednouri, and A. Issakhov. Analysis of 3E (Energy-Economical-Environmental) for Biogas Production from Landfill: A Case Study. International Journal of Chemical Engineering. 2022 (2022).

[33] K. Seshadri, A. Berlad, and V. Tangirala. The structure of premixed particle-cloud flames. Combustion and flame. 89 (1992) 333-42.

[34] J. Daou. Strained premixed flames: Effect of heat-loss, preferential diffusion and reversibility of the reaction. Combustion Theory and Modelling. 15 (2011) 437-54.

[35] S. Bakanov. The thermophoresis of solids in gases. Journal of applied mathematics and mechanics. 5 (2005) 767-72.

[36] O.-S. Han, M. Yashima, T. Matsuda, H. Matsui, A. Miyake, and T. Ogawa. A study of flame propagation mechanisms in lycopodium dust clouds based on dust particles' behavior. Journal of Loss Prevention in the Process Industries. 14 (2001) 153-60.

[37] T. Skjold. Review of the DESC project. Journal of Loss Prevention in the Process Industries. 20 (2007) 291-302.